Applying Continuous Wavelet Transforms to the Study of Variable Astrophysical Masers

Samuel Bonin
Department of Mathematics & Statistics
Thesis Advisor: Dr. Helen Wearing
Primary Investigator: Dr. William Barott

ABSTRACT

53 observations of 6.7 GHz methanol masers (microwave analogs of lasers) were taken by the Allen Telescope Array between July 2010 and January 2011. Previous research by Weisberg *et al*. (2005) has shown that maser variability on the order of milliseconds can be caused by pulsar stimulation. We found short timescale variability on the order of minutes or less in 3 of our observations. To analyze the structure of this variability we are applying Continuous Wavelet Transforms (CWTs) to the two-dimensional time series of each variable maser observation. Wavelet analysis can be thought of as a generalization of Fourier analysis that allows us to examine changes in signals over time [Lau and Weng 1995]. This paper will begin with a general overview of astrophysical masers and why we study them. Following this, there will be a description of the instrumentation used, data structure analyzed, and the techniques employed to analyze the maser data. A step-by-step summary of the analysis of G12.68 will conclude the paper. An appendix is included for additional results, including the response of CWTs to observation error.

MOTIVATION

MASER stands for Microwave Amplification by Stimulated Emission of Radiation. Analogous to more familiar optical LASERs (Light Amplification by Stimulated Emission of Radiation), masers can be created in both laboratory settings and found naturally in space [Elitzur 1992, Harwit 2006]. Astrophysical masers occur when there is a population inversion of an interstellar gas, resulting in more excited molecules in the cloud than molecules in the ground state. This state

will cause more photons to be emitted from the gas than absorbed. A process like this must be maintained by some kind of pumping action, like a source of stimulating photons. The emitted radio waves from the maser will be of the same frequency as the pumping source, as well as being coherent and of the same polarization. As a result, astrophysical masers are very powerful, with the number of emitted photons exponentially increasing with distance traveled through the source. Masers can be found in many environments, ranging from interstellar dust clouds to the so called "megamasers" at the core of active galaxies [Harwit 2006].

Masers can display variability on a wide variety of timescales: on the order of months all the way down to milliseconds [Harwit 2006, Weisberg *et al.* 2005]. Little is known about the cause of maser variability, though Weisberg *et al.* (2005) observed millisecond timescale pulsation in a hydroxyl maser. They confirmed that stimulating light from a pulsar caused this regular variability. Pulsars are extremely small, massive, and incredibly dense balls of degenerate neutrons left over after the death of a star. Due to conservation of momentum from the death of the parent star, their small size, and high mass allow for extremely fast rotation with periods of less than ten seconds to as low as several milliseconds. This also causes a powerful magnetic field that "beams" radiation from an off-axis pole, causing the observed pulsation [Harwit 2006].

Additionally, the ability of masers to greatly amplify microwaves with such fine regularity is of interest to Search for Extraterrestrial Intelligence (SETI) research. In 1993, Dr. Jim Cordes suggested that masers could be used to amplify

interstellar signal strength, and would therefore be interesting targets for SETI searches [Cordes 1993].

INTENT

53 radio observations of methanol masers were taken by the SETI Institute's radio telescope, the Allen Telescope Array (ATA), between July of 2010 and January of 2011. The intent was to find short-term variability (caused by pulsars or other pumping mechanisms), so observation lengths range from about ten minutes to as long as one hour. Of these 53 observations, only three were found to be variable. The three variable masers are G49.49, G23.01, and G12.68. G49.49 and G23.01 were found to be variable in the summer of 2010 by Dr. Barrot's previous REU student. G12.68 was found to be variable in the summer of 2011 by Dr. Barrot and I, and a later observation of G49.49 was confirmed to be variable as well. Only one observation of G23.01 is available for study, and a previous observation of G12.68 is questionably variable. Due to funding problems, the ATA was shut down shortly before research for this project began in the summer of 2011, and follow up observations have not been taken.

ANALYSIS TECHNIQUES

Fourier Analysis

In order to study the structure and periodicity of masers, we use several techniques that have been developed to analyze time series data. Initially, we used Fourier analysis, which works with the knowledge that any aperiodic continuous

time series *x(t)* can be expressed in terms of an infinite number of sinusoidal functions of frequency *f* such that:

$$x(t) = \int_{-\infty}^{\infty} \hat{x}(f)\, e^{i2\pi f t} df \qquad (1)$$

Where $\hat{x}(f)$ is some function of frequency [Brigham and Morrow 1967]. Due to the orthonormality of $e^{-i2\pi f_1 t}$ and $e^{i2\pi f_2 t}$ for all frequencies f_1 and f_2, we can take the *Fourier Transform* of *x(t)* such that:

$$\hat{x}(f) = \int_{-\infty}^{\infty} x(t) e^{-i2\pi f t} dt \qquad (2)$$

thus finding the *Fourier Coefficient* for every frequency *f* [Brigham and Morrow 1967, Woyczynski 2011]. For the purposes of computation, we can take a discretized time series x_n with *N* time steps t_n such that the *Discrete Fourier Transform* (DFT) is formulated as follows:

$$\hat{x}_n = \delta t \sum_{n'=0}^{N-1} x_{n'}\, e^{-i2\pi n n'/N} \qquad (3)$$

where $\delta t = \frac{t_N}{N}$ is the length of one time step. The power at a given frequency $\frac{n}{t_N}$ is given by $|\hat{x}_n|^2$, allowing us to create a periodogram of the transform [Brigham and Morrow 1967, Woyczynski 2011]. This periodogram is made using a Fast Fourier Transform (FFT) in MATLAB (the FFT being a more efficient method of computing a DFT) [Sauer 2006]. An example of the use of this method is given in Figure 1.

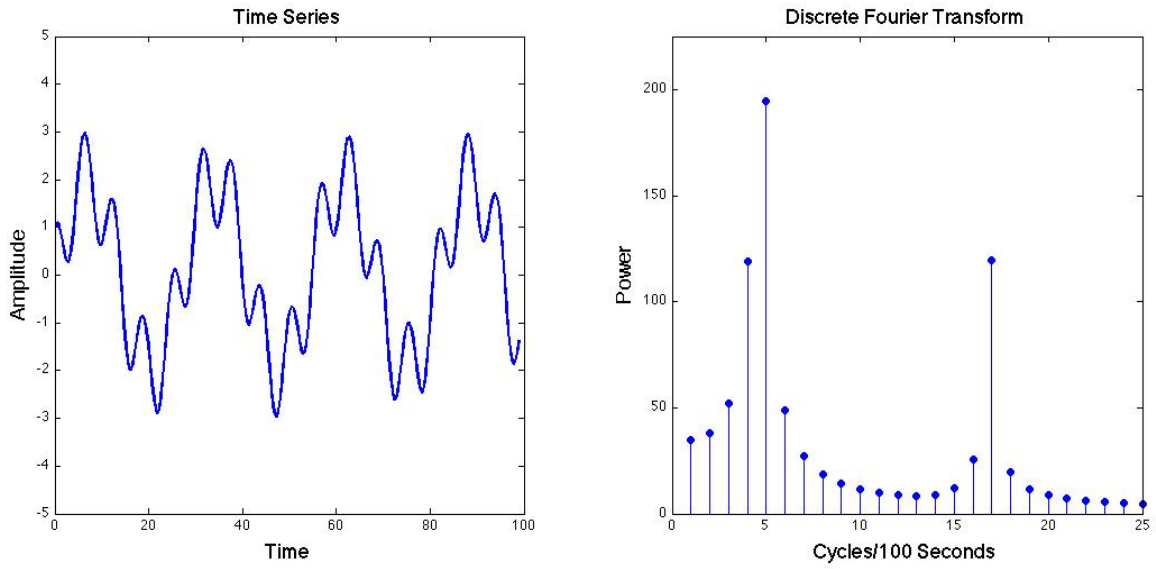

Figure 1: Here the DFT is computed for a finite-length time series consisting of a function with two summed periodic components. Notice the spectral leakage around the two main frequencies in the periodogram.

Fourier analysis, however, has its limitations. One notable problem concerns a phenomenon known as spectral leakage, which is well illustrated in Figure 1. Due to the fact that we are sampling a finite number of frequencies and have a finite amount of data, most frequencies will not be periodic within the given "data window." As a result, frequencies tend to be smeared in the periodogram (even if there are only a finite number of frequencies present, as is the case in Figure 1) [Harris 1978, Scargle 1982]. In practice, Fourier analysis allows for quick identification of variability in a time series, but provides no information concerning the location of that frequency in time. This problem can be solved, in part, by the use of Windowed Fourier Transforms (WFTs), in which we only look at successive windows of a given time series, allowing us some insight into the dynamics of the variability. However, WFTs have their own inherent problems introduced by the window itself, such as the size of the window ultimately determining those

frequencies that are accurately analyzed. WFTs will preferentially pick out higher frequency variability due to the low number of cycles of low variability in a short window [Lau and Weng 1995]. For these maser analyses, we made no use of WFTs.

Wavelet Analysis

The advantage of Continuous Wavelet Transforms (CWTs) over both of the previous techniques lies in the fact that they are more localized in time and frequency [Torrence and Compo 1998]. In the analysis of variable masers, variability can be on timescales as short as milliseconds and as long as significant fractions of the observation time (which, in this case, tends to be around 1 hour for the best observations). A WFT would struggle to pick out these frequencies at the extremes of sampling frequency and observation length, making the use of CWTs ideal.

"A (CWT) uses generalized local base functions (wavelets) that can be stretched and translated with a flexible resolution in both frequency and time [Lau and Weng 1995]." By dilating the wavelet and shifting its location along the time series, we are able to extract information both about frequencies present in the time series and how they change in time [Torrence and Compo 1998]. The Heisenberg Uncertainty Principle states:

$$\sigma_p \sigma_f \geq C \quad (4)$$

where σ_p and σ_f are the variance of the position and frequency of some periodic function, respectively, and C is some constant. Consequently, the better we know the location of a particular frequency in a time series, the less certain we are about

its actual frequency [Selig 1995]. When using a CWT, higher frequencies have less localization in frequency, whereas low frequencies have less localization in time [Le and Argoul 2003, Lau and Weng 1995].

While many wavelets can be used, for the purposes of maser analysis we will use the "Morlet" wavelet (a sinusoid modulated by a Gaussian), which is described as follows:

$$\psi_0(\eta) = \pi^{\frac{-1}{4}} e^{i\omega_0\eta} e^{\frac{-\eta^2}{2}} \quad (5)$$

The constant ω_0 is equal to 6 to ensure that the wavelet has "zero mean and (is) localized in both time and frequency space" [Torrence and Compo 1998]. The Morlet wavelet is ideal for our analysis due to its periodic nature, and our knowledge that periodic behavior has been oberserved in masers. See Figure 2 for a sample Morlet Wavelet.

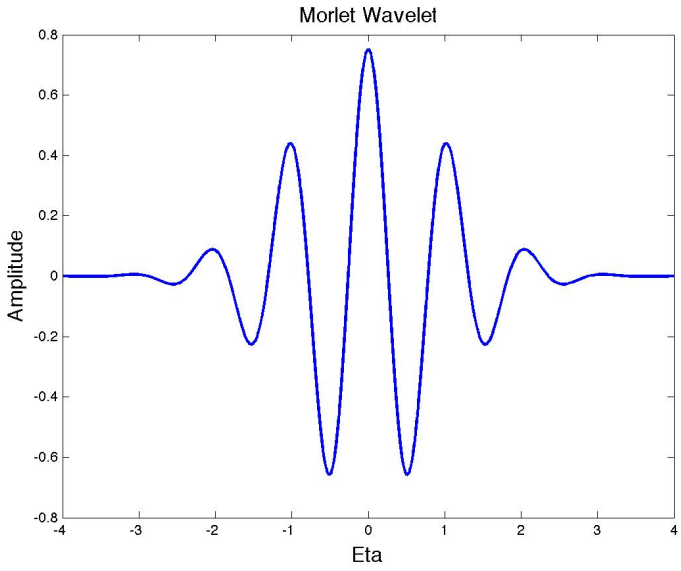

Figure 2: A sample Morlet wavelet.

The CWT itself is shown in equations 6 and 7, where $x_{n'}$ is the time series, $\psi_0^*(\eta)$ is the complex conjugate of the Morlet wavelet, *s* is the scale, and δt is the length of one time step in a time series containing *N* time steps [Grinsted *et al.* 2004, Torrence and Compo 1998, Lau and Weng 1995]. The term in front of the integral and summation, respectively, normalizes the wavelet so that its integral with respect to frequency is equal to 1. For the purposes of computation the latter discrete formulation is used (equation 7).

$$W_n(s) = \frac{1}{s}\int x_{n'}\,\psi_0^*\left(\frac{n'-n}{s}\right)dn' \qquad (6)$$

$$W_n(s) = \frac{\delta t}{s}\sum_{n'=0}^{N-1} x_{n'}\,\psi_0^*\left[(n'-n)\frac{\delta t}{s}\right] \qquad (7)$$

It is faster to compute the CWT if we take the DFT of the time series and wavelet. In equation 8[1], $\hat{x}_k$ is the DFT of the time series, and $\hat{\psi}_0$ is the normalized DFT of the wavelet such that it follows equation 9 [Torrence and Compo 1998].

$$W_n(s) = \sum_{k=0}^{N-1} \hat{x}_k\,\hat{\psi}_0^*\,(s\omega_k)e^{i\omega_k n\delta t} \qquad (8)$$

$$\int_{-\infty}^{+\infty}\left|\hat{\psi}_0(\omega')\right|^2 d\omega' = 1 \qquad (9)$$

Edge effects still must be taken into account. To indicate where discontinuities at each end of the time series play a significant role in the CWT, a cone of influence

[1] Equation 1 may also be formulated as follows: $x(t) = \frac{1}{2\pi}\int_{-\infty}^{\infty}\hat{x}(\omega)e^{i\omega t}d\omega$ [Brigham and Morrow 1967].

(COI) is shown in each CWT plot (the shaded region in Figure 3). This is calculated using what is known as the *e*-folding time, where "the wavelet power for a discontinuity at the edge drops by a factor e^{-2} and ensures that the edge effects are negligible beyond this point [Torrence and Compo 1998]." For the Morlet wavelet, the *e*-folding time is $s\sqrt{2}$ [Torrence and Compo 1998]. See Figure 3 for a demonstration of the CWT.

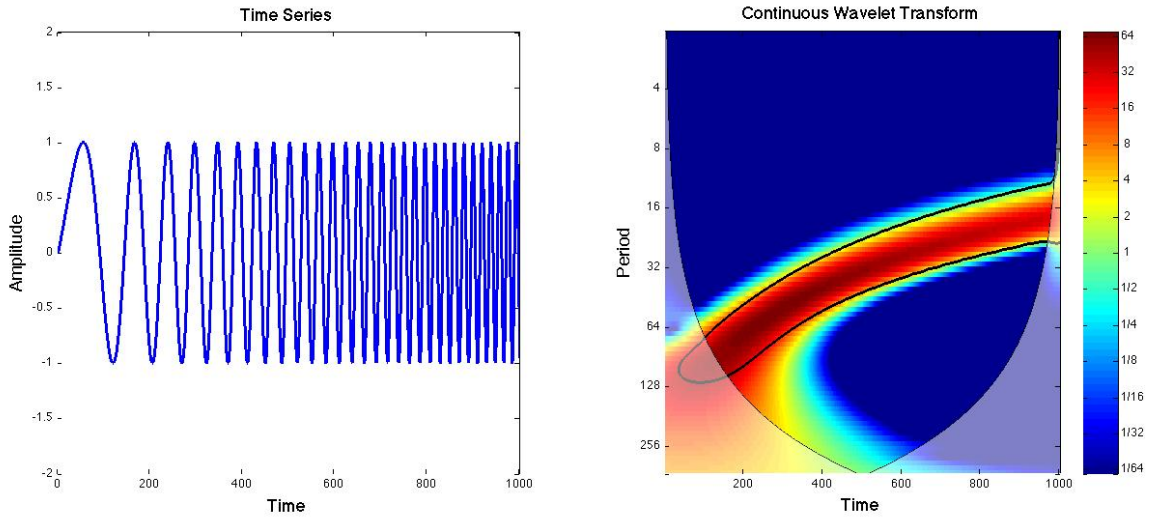

Figure 3: The CWT of a time series containing periodicity of increasing frequency. The shaded area in the CWT is the COI.

Wavelet Coherence

Another useful tool for the study of variable masers is called Wavelet Coherence (WC). Displayed in a similar way to a CWT, WC quantifies the level of correlation between two time series. Frequencies that are exactly in phase and perfectly out of phase will show the same power in the WC, so the relative phase is computed as well to make the correlation more clear. This method utilizes the cross wavelet spectrum (CWS) (showing high common power between two time series [Grinsted *et al*. 2004]), which is defined by the equation:

$$W_n^{XY}(s) = W_n^X(s)W_n^{Y*}(s) \qquad (10)$$

The star again indicates the complex conjugate. WC is defined as:

$$R_n^2(s) = \frac{\left|S\left(s^{-1}W_n^{XY}(s)\right)\right|^2}{S(s^{-1}|W_n^X(s)|^2) \cdot S(s^{-1}|W_n^Y(s)|^2)} \qquad (11)$$

where we square the CWT and normalize it by the square of each transform [Grinsted *et al.* 2004, Torrence and Compo 1998]. Grinsted *et al.* (2004) note that this function looks very much like a correlation coefficient. The operator S smooths the given transform across time and scale. This is necessary, otherwise $R_n^2(s)$ would equal 1 everywhere [Torrence and Compo 1998]. The smoothing operators depend entirely on the wavelet used, and, using the rectangle function Π, those for the Morlet wavelet are given in the following equations [Grinsted *et al.* 2004]:

$$S(W) = S_{scale}\left(S_{time}\left(W_n(S)\right)\right) \qquad (12)$$

$$S_{time}(W)|_s = \left(W_n(S) * c_1 e^{\frac{-t^2}{2s^2}}\right)\Big|_s \qquad (13)$$

$$S_{scale}(W)|_s = \left(W_n(S) * c_2 \Pi(0.6s)\right)\Big|_s \qquad (14)$$

The constants c_1 and c_2 normalize the equations such that they "have a total weight of unity" [Torrence and Webster 1998]. The scalar 0.6 was empirically determined for scale averaging and is known as the "scale decorrelation length" [Torrence and Compo 1998, Torrence and Webster 1998]. WC is demonstrated in Figure 4. All

CWT and WC plots were made using Dr. Aslak Grinsted's MATLAB wavelet analysis package (http://www.pol.ac.uk/home/research/waveletcoherence/).

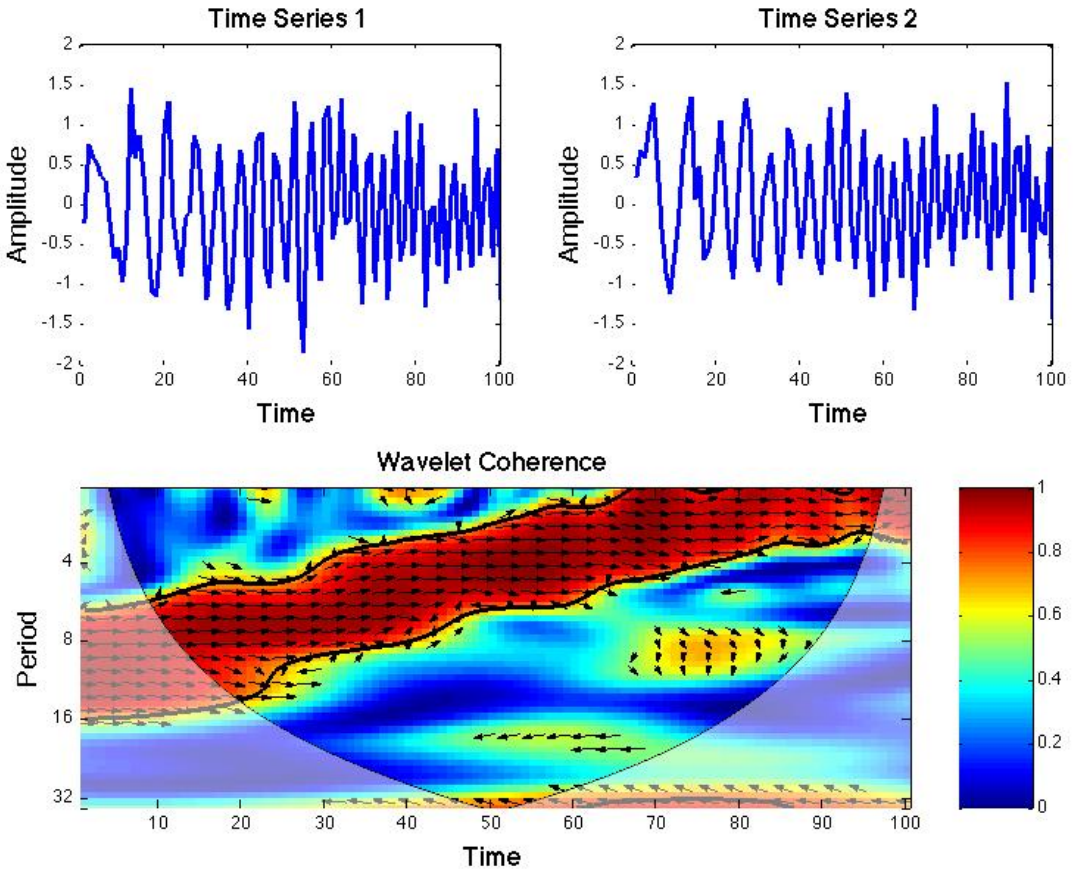

Figure 4: WC is applied to two time series containing the same periodic variability seen in Figure 2, yet different patterns of noise. The more to the right an arrow is pointing, the more in phase the two time series are at that point in time and scale. Had the time series been identical, the WC plot would have been red at all times and scales, in addition to being completely in phase.

APPLICATION OF WAVELET ANALYSIS TO THE STUDY OF METHANOL MASERS

In order to demonstrate how variability is found in maser observations, the step-by-step process for the variable maser G12.68 will now be illustrated. Results for the other two variable masers (G49.49 and G23.01) are included in the appendix.

Data gathered from the ATA is collected in extremely large binary files (about 10-50 GB in size), which are reduced in MATLAB to matrices whose file size

depends upon the desired resolution. All observation matrices in this paper were reduced to 1-second resolution with 8000 microwave emission frequency channels. Emission frequency and wavelength are directly analogous for electromagnetic radiation, since all light travels at a constant velocity in a vacuum. For clarity, these channels will be referred to as wavelength channels, in order to avoid confusion when referring to changes in time series periodicity.

After reduction, the observation is visually inspected at a single interval in time. Should the maser signal be powerful enough for short integration times (1 second or less), the maser is selected for further analysis. Using a plot called a "Waterfall," we can construct the two dimensional time series for the entire observation. Both the power versus wavelength plot and waterfall for G12.68 are shown in Figure 5 and Figure 6, respectively.

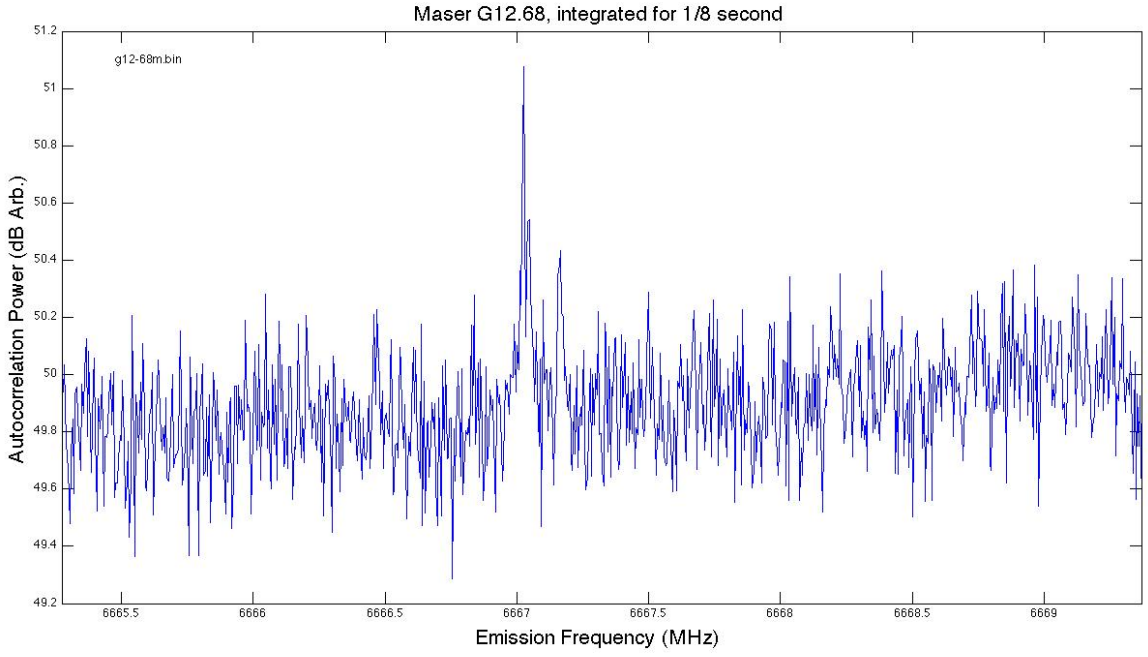

Figure 5: While the analysis of G12.68 was conducted at 1 second time-resolution, this plot used a 1/8 second integration time rather than 1 second (for clarity).

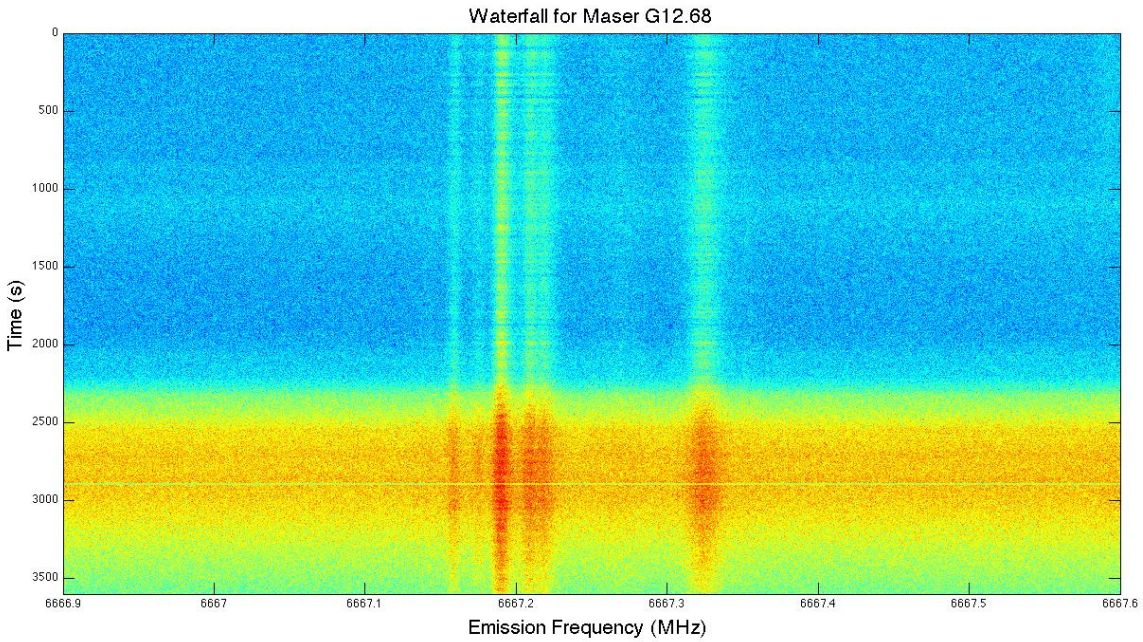

Figure 6: A waterfall is the two dimensional time series for a given observation. Redder coloration shows higher power. A time series at a specific wavelength (emission frequency) is called a "channel." This particular observation contains several "maser lines," which we will later show to be coherent. The horizontal line across wavelengths near 3000 seconds is an observation error, and the increase in power across wavelengths starting at around second 2250 is likely natural. The sun rising during the observation could cause this power change.

Inspection of the waterfall reveals which channels the maser is located in. The maser is frequently split between multiple lines, as is the case for G12.68. This phenomenon can be caused by observation of multiple masers or magnetic fields (this is known as Zeeman splitting) [Harwit 2006]. Visual inspection of the waterfall can also show variability, as is evident in the "stratification" of the maser lines in the waterfall in Figure 6.

Additionally, we may take the Signal Plus Noise-to-Noise Ratio (SNNR) of several binned channels and visually inspect the resulting time series. "Binning" channels involves adding sequential channels together in order to amplify any variability that may be present. The SNNR is then taken in the following manner:

$$SNNR_t = \frac{S_t + N_{1,t}}{N_{2,t}} \quad (15)$$

where S_t is a time series consisting of several binned maser channels (from a single maser line), and $N_{1,t}$ and $N_{2,t}$ are time series consisting of different sequentially binned noise channels taken from the observation. See Figure 7 for the SNNR of G12.68.

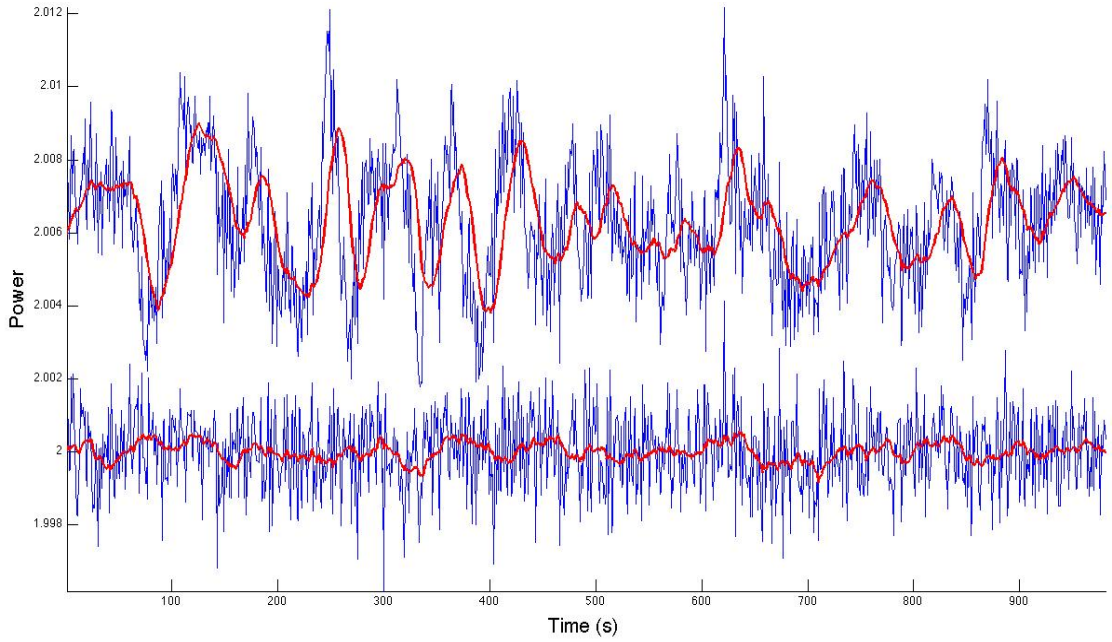

Figure 7: SNNR of binned channels from G12.68. The function in red is a filter (the MATLAB filter function *filter.m*) using a window of 20 seconds. The fluctuations of the maser line are much larger than that of the noise channels.

Additionally, we compute the FFT along each channel and plot the resultant two-dimensional periodogram (see Figures 8 and 9). Inspection of both the time series and the FFT reveals variability in the maser.

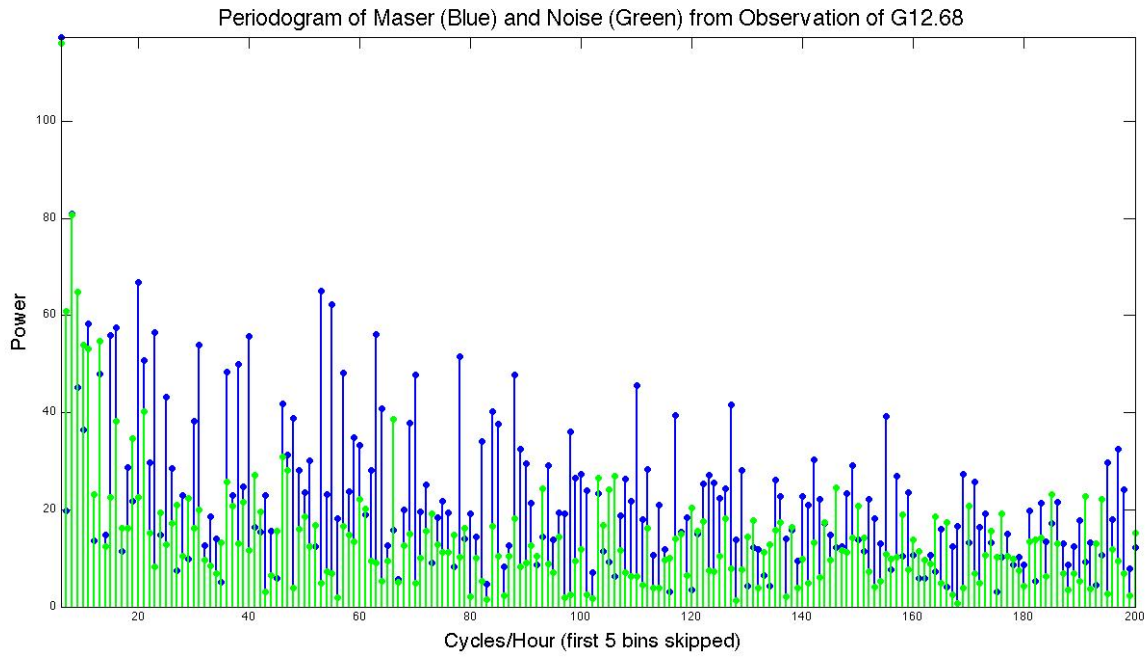

Figure 8: This periodogram of the maser and observation noise from G12.68 clearly shows variability that is inherent to the maser line. Both periodograms were calculated from the FFT of a single noise or maser channel.

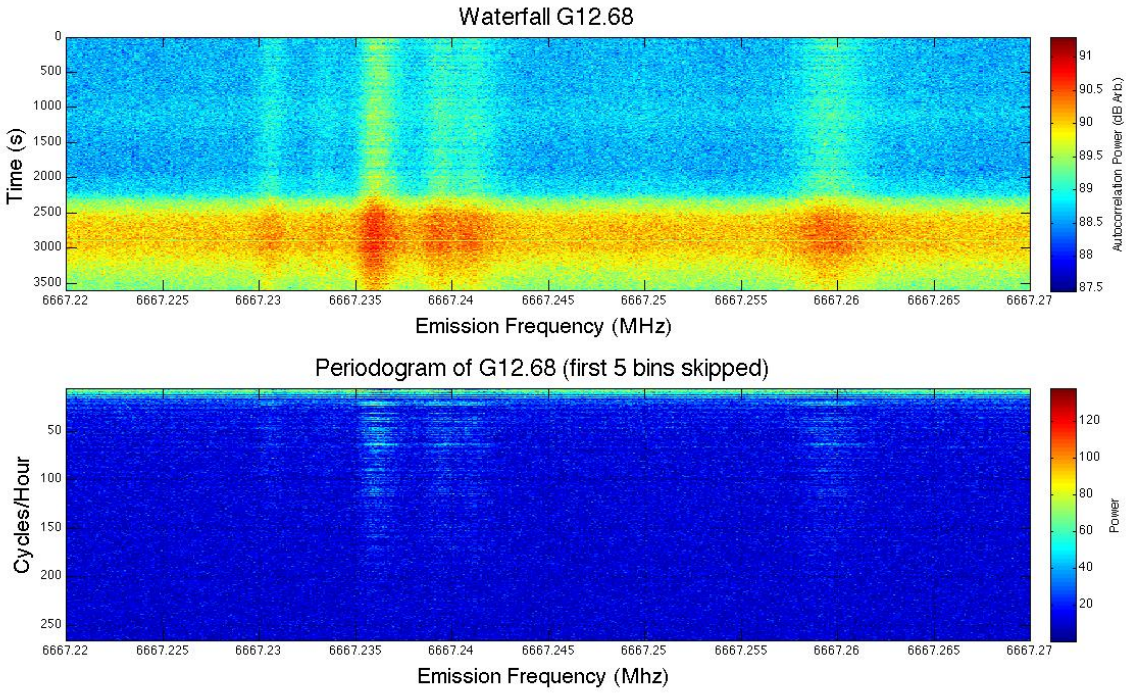

Figure 9: The 2-dimensional periodogram of G12.68 illustrates that variability is present in multiple maser lines.

Application of the CWT will reveal the structure of that variability. We apply the CWT to several binned masers channels and noise channels. If there is a significant difference in variability between the two, the variability found using the FFT and SNNR is confirmed. Figure 10 is the CWT of one maser line from G12.68.

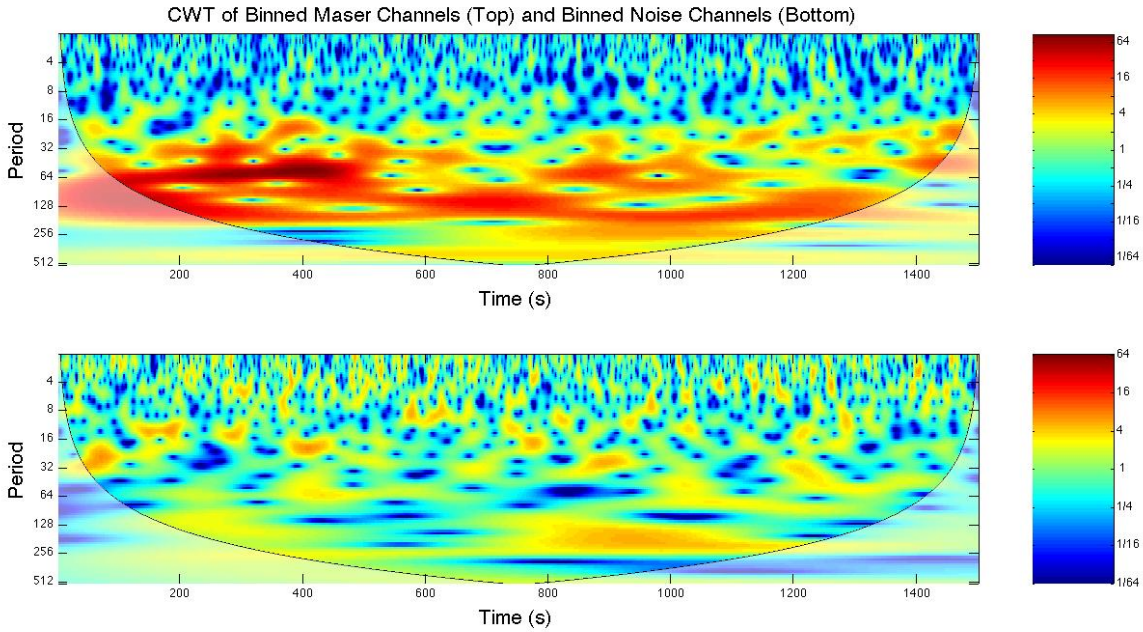

Figure 10: Significant change in maser variability is clear, particularly at Period 64 between 200 and 400 seconds into the observation. It is also clear from the bottom CWT that this variability is not caused by noise.

If variability is confirmed with the CWT, WC is applied. Either one maser line is split down the center, binning those two sets of channels from the same line, or two different binned maser lines are compared. In the case of G12.68, two maser lines were analyzed.

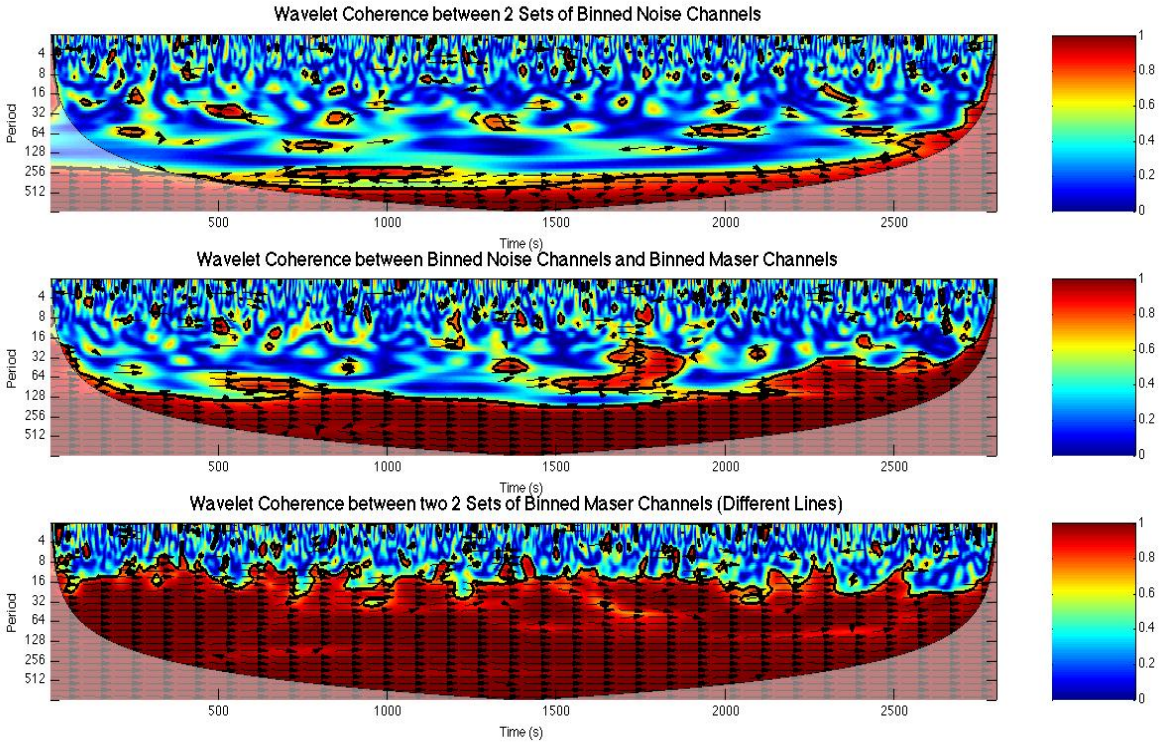

Figure 11: Maser-Noise and Noise-Maser WC shows low-frequency coherent variability, likely due to the large power change across frequency present at the end of the observation. Maser-Maser WC shows significant coherence down to a wavelet period of ~16 seconds, illustrating that the two maser lines are variable, coherent, and possibly pumped by the same source. You may have noticed that neither the CWT from figure 10 nor WC was applied to the entire length of the observation. This is due to the error in the observation, and will be discussed in the appendix.

CONCLUSIONS

While variability has been previously confirmed, it has been restricted to studies of highly periodic, high frequency variability, or extremely long term variability. This is the first time Wavelet Analysis has been applied to the study of masers, confirming our observations of variability on the order of minutes or less in 3 of our observations. If one's goal were to construct a catalog of variable masers, FFTs and SNNR techniques would likely be sufficient. However, CWTs are

invaluable for examining the structure of the variability present in the maser lines. Additionally, WC is incredibly useful for verifying that multiple maser lines are coherent, provided that their respective observations are co-temporal. Additionally, WC provides insight into the broad-spectrum variability of a maser, again, provided that we have co-temporal coherent time series. Due to these two conclusions concerning the use of the WC method, the WC is a more useful tool than the CWT alone.

Future work hopefully involves further observations with the ATA, which has since been taken out of hibernation via public donations. We wish to catalog as many variable masers as we can in order to facilitate further study of this phenomenon. It may be possible that Wavelet Analysis, and particularly Wavelet Coherence, can be applied to observations of both a maser and possible pumping sources associated with that maser. This would be an invaluable technique for the identification of aperiodic pumping sources.

ACKNOWLEDGEMENTS

I would like to thank Dr. Helen Wearing and Christian Gunning of UNM for years of technical advice, mentorship, encouragement, and the inspiration to study wavelet analysis. I would also like to thank Dr. William Barott of Embry-Riddle Aeronautical University, without whom I would never have worked on this project, for his mentorship and a fantastic REU experience. Both the SETI Institute and National Science Foundation Grant AST0852095 supported this project.

APPENDIX

WAVELET COHERENCE RESPONSE TO OBSERVATION ERROR

Observation error presents a unique challenge when using CWTs and WC. Near second 2900 of the observation for G12.68, there is a sudden drop in power, across wavelengths, for a few seconds. Additionally, the power during this interval is not constant. In practice, one can account for this by placing appropriately averaged values in the time series. Unfortunately, some information, however insignificant, is still preserved in this power change. Since this observation of G12.68 is long, and only contains one error, it is appropriate to just ignore the last 800 seconds of the observation. However, some observations contain two or more errors spread out through the entire observation, necessitating a different method for compensation.

The effects of the power change on the CWT and WC are illustrated in Figures 12 and 13, respectively. Smaller scale wavelets will not pick up the power change unless they are very close to it, while larger wavelets pick it up farther away. Consequently, observation errors tend to obscure possible variability at lower frequencies.

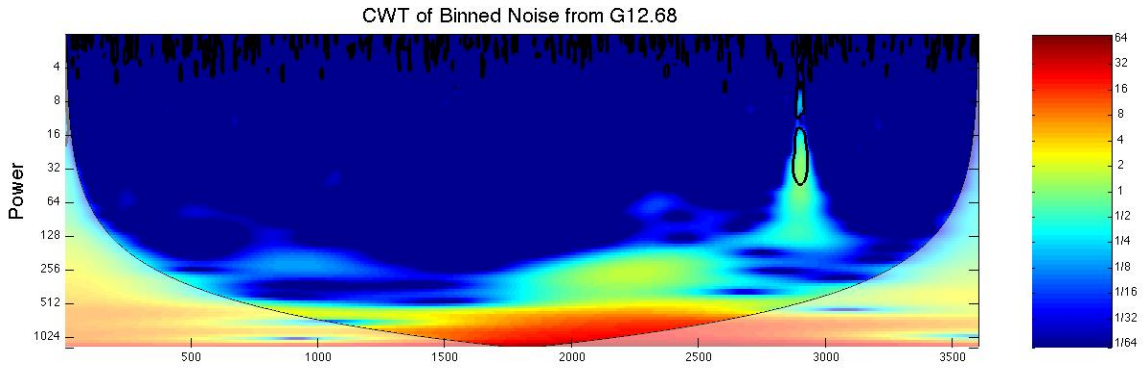

Figure 12: CWT of noise from G12.68 easily picks out the observation error.

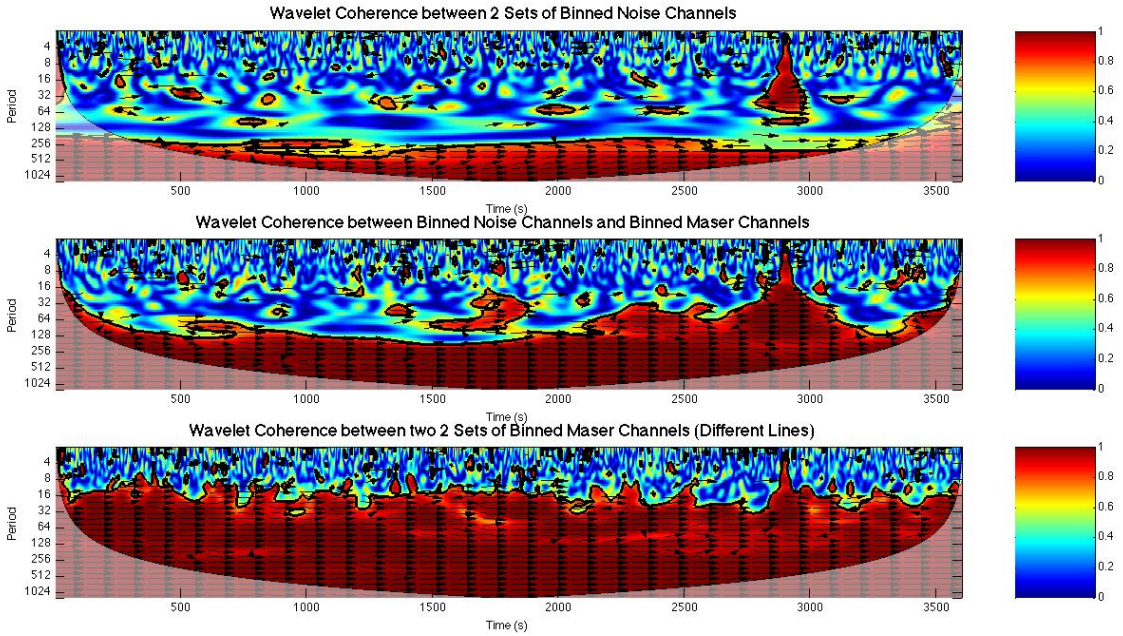

Figure 13: The effects of observation error are more pronounced with WC, where coherence at lower frequencies, or a lack thereof, could be hidden.

WAVELET ANALYSIS RESULTS FOR MASER G49.49

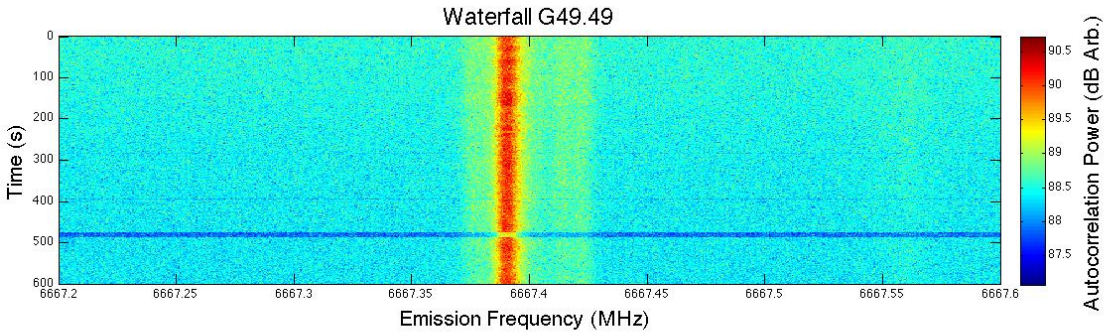

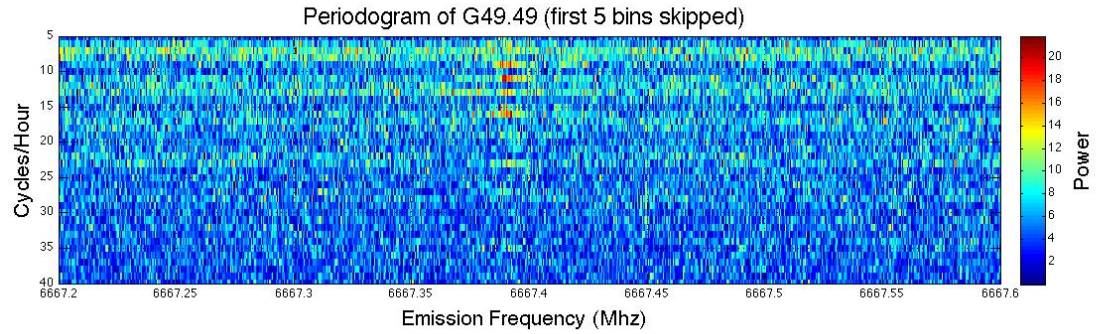

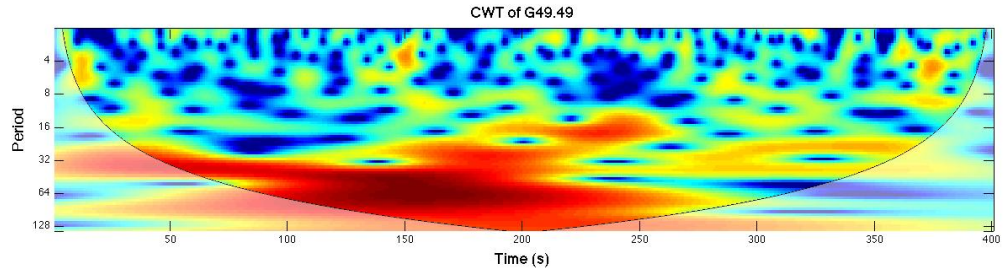

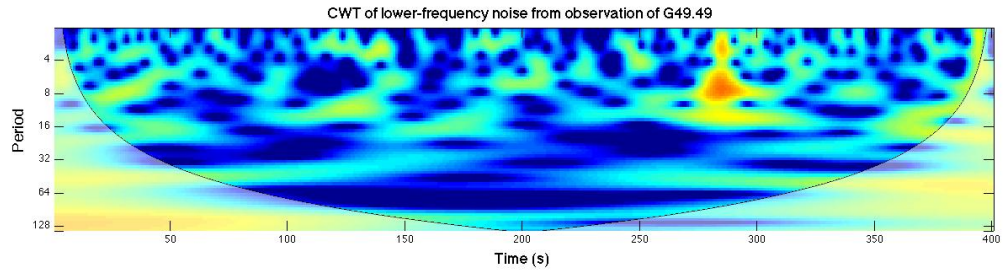

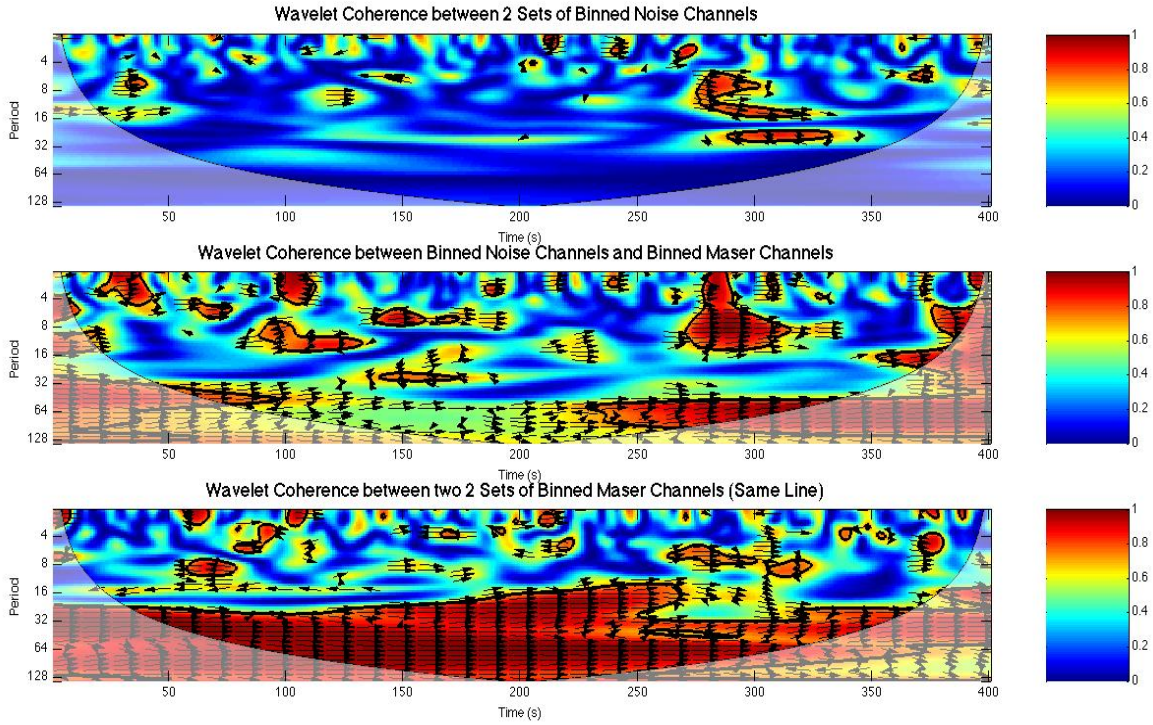

WAVELET ANALYSIS RESULTS FOR MASER G23.01

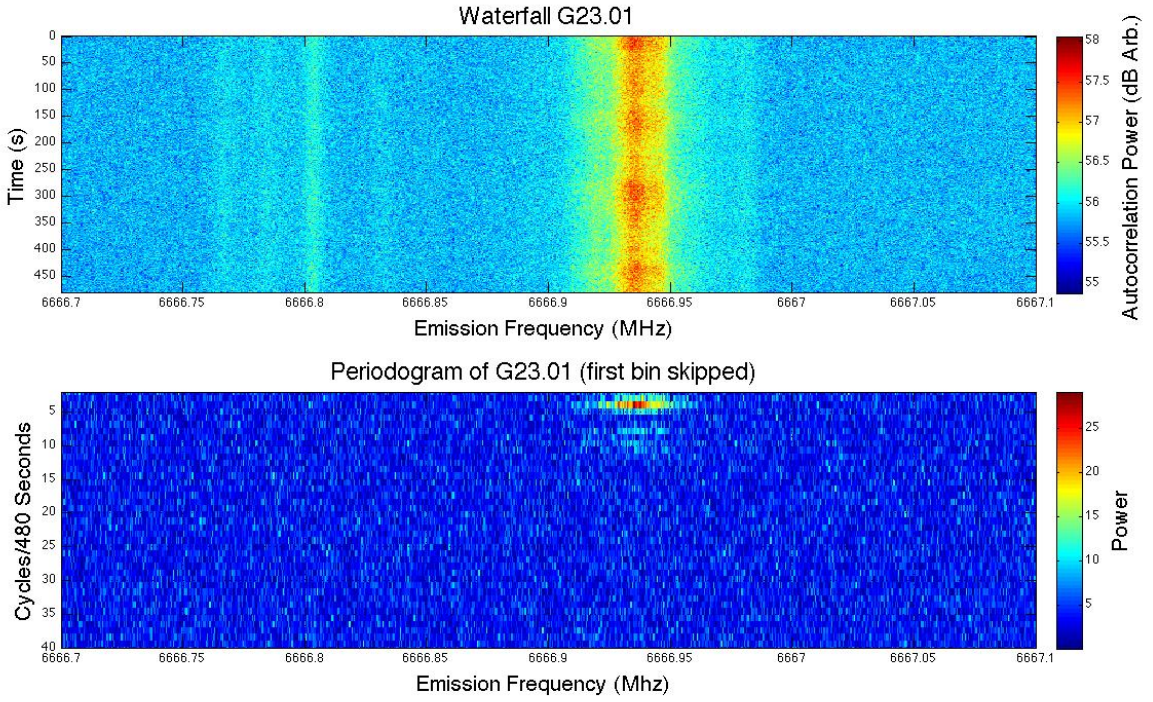

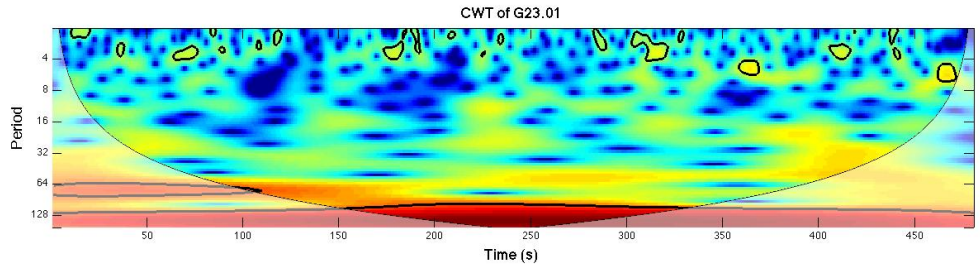
CWT of G23.01
Period
4
8
16
32
64
128
50
100
150
200
250
300
350
400
450
Time (s)

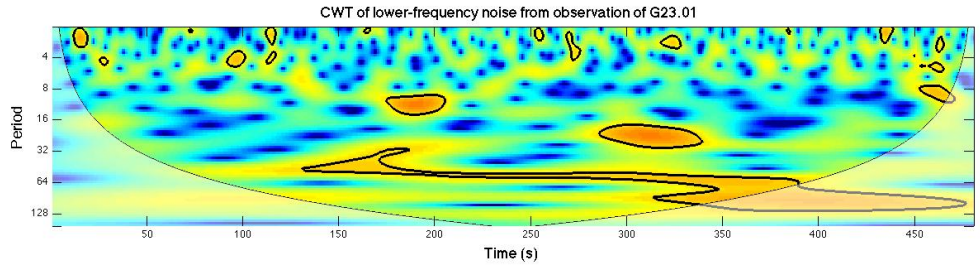
CWT of lower-frequency noise from observation of G23.01
Period
4
8
16
32
64
128
50
100
150
200
250
300
350
400
450
Time (s)

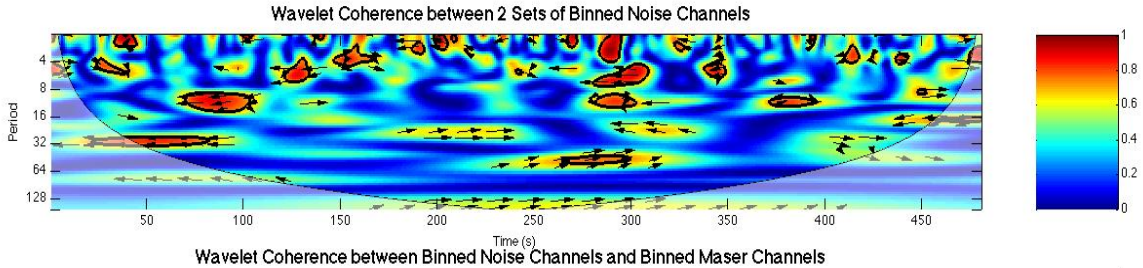
Wavelet Coherence between 2 Sets of Binned Noise Channels
Period
4
8
16
32
64
128
50
100
150
200
250
300
350
400
450
Time (s)
1
0.8
0.6
0.4
0.2
0

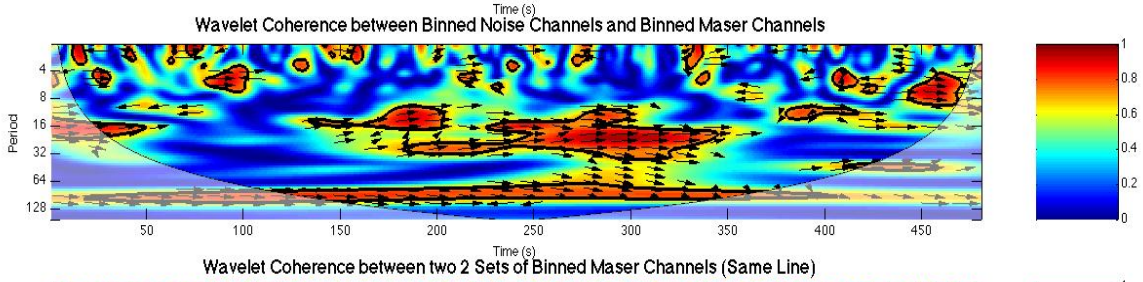
Wavelet Coherence between Binned Noise Channels and Binned Maser Channels
Period
4
8
16
32
64
128
50
100
150
200
250
300
350
400
450
Time (s)
1
0.8
0.6
0.4
0.2
0

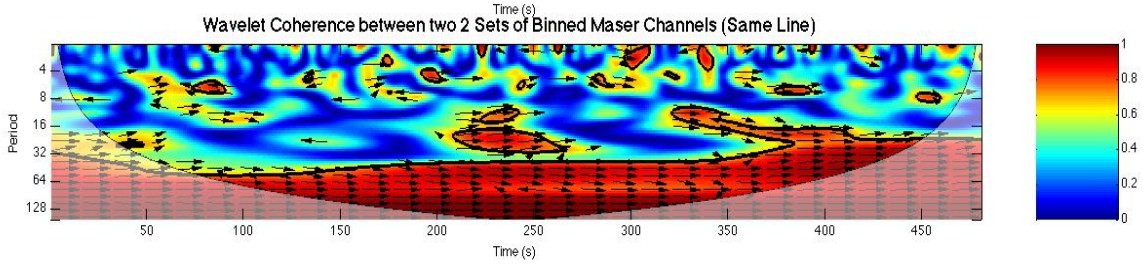
Wavelet Coherence between two 2 Sets of Binned Maser Channels (Same Line)
Period
4
8
16
32
64
128
50
100
150
200
250
300
350
400
450
Time (s)
1
0.8
0.6
0.4
0.2
0

WORKS CITED

Brigham, E. O. and Morrow, R. E. (1967): The fast Fourier transform. *Spectrum, IEEE*, vol.4, no.12, pp.63-70.

Cordes J. M. (1993): *Astron. Soc. Pacific Conf. Series*, 47, 257.

Elitzur, M. "Astronomical Masers." Kluwer Academic Publishers, 1992.

Grinsted, A. *et al.*, (2004): Application of the cross wavelet transform and wavelet coherence to geophysical time series. *Nonlinear Processes in Geophysics* 11, 5/6 561-566.

Harris, F.J., (1978): On the use of windows for harmonic analysis with the discrete Fourier transform. *Proceedings of the IEEE* , vol. 66, no. 1, pp. 51- 83.

Harwit, Martin. "Astrophysical Concepts, Fourth Edition." Springer, 2006.

Lau, K-M., Weng, H. (1995): Climate Signal Detection Using Wavelet Transform: How to Make a Time Series Sing. *Bull. Amer. Meteor. Soc.*, 76, 2391–2402.

Le, T-P. and Argoul, P., (2004): Continuous wavelet transform for modal identification using free decay response, *Journal of Sound and Vibration*, Volume 277, Issues 1–2, pp. 73-100.

Sauer, T. "Numerical Analysis." PEARSON Addison Wesley, 2006.

Scargle, J. D., (1982): Studies in astronomical time series analysis. II – Statistical aspects of spectral analysis of unevenly spaced data. *Astrophysical Journal*, Part 1, vol. 263, pp. 835-853.

Selig, K., (1995): Trigonometric Wavelets and the Uncertainty Principle. *Mathematical Research*, vol. 86, pp. 293-304.

Torrence, C. and Compo G. P., (1998): A Practical Guide to Wavelet Analysis. *Bull. Amer. Meteor. Soc.*, 79, 61–78.

Torrence, C. and Webster, P. J., (1998): The annual cycle of persistence in the El Niño/Southern Oscillation. *Q.J.R. Meteorol. Soc*., 124: 1985–2004.

Weisberg, J. M. *et al.*, (2005): Discovery of Pulsed OH Maser Emission Stimulated by a Pulsar. *Science*, 309, 5731.

Woycznski, W. A. "A First Course in Statistics for Signal Analysis." Birkhäuser Boston, 2011.